2016

Effect of End Plates on Heat Transfer of Plate Heat Exchanger

Shenghan Jin
University of Illinois, United States of America, sjin8@illinois.edu

Pega Hrnjak
pega@illinois.edu

Effect of end plates on heat transfer of plate heat exchanger

Shenghan Jin[1], Pega Hrnjak[1,2,*]

[1]Air-Conditioning & Refrigeration Center
University of Illinois at Urbana-Champaign, 1206 West Green Street, Urbana, IL, USA
sjin8@illinois.edu, pega@illinois.edu

[2]Creative Thermal Solutions, Inc. (CTS), Urbana, IL, USA

[*]Corresponding author

ABSTRACT

Steady-state heat transfer data for single-phase (water) in both frame-and-plate (FPHE) and brazed plate heat exchangers (BPHE) are presented with various number of chevron plates in U-type flow arrangement. Analysis of the experimental results indicates that the end plates, instead of being adiabatic, function as fins due to the contact with adjacent plates. The experimental data is used to validate a thermal conduction model in ANSYS, which indicates that the end plates fin efficiency is a function of fluid convective heat transfer coefficient and conductive thermal resistance. In the frame-and-plate heat exchanger, the pressing force of the frame may affect the contact thermal resistance, thus change the fin efficiency. In brazed plate heat exchanger, the fin efficiency is much higher due to the larger contact area and higher conductivity of the brazing material. Although the effect of end plates is quickly diluted by the increased number of plates in real applications, it could be significant when plate number is small, as is often the case in laboratory settings for the development of heat transfer correlations.

1. INTRODUCTION

Frame and plate heat exchanger (FPHE) is commonly used for their ease of cleaning, simple adjustment of heat transfer area, compactness and excellent thermal-hydraulic performance [1]. It essentially consists of multiple thin metal plates that are stamped with a wavy chevron or herringbone pattern. Fluid channels are formed by pressing the plates with opposite chevron direction together. The alternating flows are directed and sealed by the gaskets in between. The contact points between crests and troughs of two adjacent plates subdivide the fluid path into an array of interconnected unitary cells, which turbulate the flow and enhance heat transfer.

Early applications of FPHE are mainly for liquid-liquid heat transfer in the lower pressure range (usually below 1.6 MPa), including dairy, pulp and paper industries for their hygiene requirements [1]. With the introduction of brazed plate heat exchanger (BPHE), such plates could withstand higher pressure and later on found its increasing application as condenser and evaporator in air-conditioning and refrigeration systems.

Numerous studies have been carried out to measure single-phase and two-phase flow heat transfer, as summarized in review articles [2] and textbooks [3]. However, only a few have investigated the effect of end plates, which are referred to as the "two outer plates" and "ideally do not transfer heat" in most of the open literatures [1][3][4]. Meanwhile most manufactures only count the interior plates, known as thermal plates, for active heat transfer area.

Nevertheless, the effect of end plates is not always trivial. For instance, Heggs and Scheidat [5] recommended 19 plates for the end plates effect to be less than 2.5%. To characterize and compensate such effect, most work in open literature have taken the method of adding a correction factor on log mean temperature difference (LMTD) or plot ε-NTU for different configurations and operating conditions. In 1961, Buonopane et al. [6] experimentally determined the correction factor F for 1pass-1pass flow arrangement with up to 17 thermal plates and multi-pass series flow arrangements with up to 11 thermal plates. In a similar manner, Foote [7], Usher [8] and Marriott [9] presented the F factor as a function of thermal plates for various configurations in the late 1960s. Jackson and Troupe [10], and Kandlikar [11] used numerical method to analyze the ε-NTU relationship in various number of plates. In 1988, a more

comprehensive study was carried out by Kandilikar and Shah [4], who investigated the influence of the number of thermal plates on plate heat exchanger performance through numerical analysis for 1pass-1pass, 2pass-1pass and 3pass-1pass flow arrangement. The correction factor F for LMTD was tabulated as a function of number of capacitance ratio R, heat transfer unit (NTU), temperature effectiveness P and number of plates N. As a result, the authors concluded that for 1pass-1pass heat exchanger, even versus odd number of thermal plates have a strong influence on the correction factor F and a negligible influence for N>40. Polley and Abu-Khader [12] followed the same path but simplified the process with a bypass model, which covered a wider range of heat exchanger capacity.

The approach of using correction factor has provided a good guideline for most practical purposes. It has covered a wide range of operating conditions and configurations, yet it treats the end plates as an engineering problem and has offered no fundamental explanations on how the end plates affect heat transfer. Therefore there could always be circumstances that find such approach insufficient. For example, the approach assumes uniform flow distribution, thus rendered inapplicable in two-phase flow where maldistribution is non-negligible, even with small number of plates. At occasions with maldistribution excluded, such as a 1pass-1pass 3-channel setup (two-phase flow in the center channel), as is often the case in two-phase heat transfer test [13][14], such method does not cover the situation of capacitance ratio R being infinity.

This paper is to propose a new explanation that end plates, instead of being treated conventionally as adiabatic, function as fins due to the contact with adjacent plates. Steady-state heat transfer data for single-phase (water) in both FPHE and BPHE with various number of plates are presented. The experimental data is used to validate a thermal conduction model in ANSYS, which incorporates plate geometries and operating conditions. It indicates that the end plate fin efficiency is a function of fluid convective heat transfer coefficient and conductive thermal resistance. The final result is in agreement with that of the correction factor approach, but provides a more fundamental explanation and general application.

2. EXPERIMENTAL APPARATUS AND PROCEDURE

2.1 Experimental apparatus

The schematics of the experimental apparatus is shown in Figure1. It consists of three independent loops: two water loops and water-glycol loop. Two magnetic driven pumps with variable frequency drives are used to circulate the deionized water for hot and cold stream loops, respectively. Expansion tank is placed at the highest location of each loop and the system is held vacuum until fully charged with water, so that no pocket of air is trapped inside.
Micromotion flow meter, absolute and differential pressure transducers, and type T (copper-constantan) thermocouples are installed at locations as indicated in Figure 1. Their range and uncertainty after calibration are listed in Table 1. As a result, the experimental uncertainty for Re, *f* and Nu are calculated through error propagation rule, with their maximum value also listed in Table 1.

Table 1: Measurement uncertainty

Measured Parameter	**Uncertainty**
Temperature (T type)	0.1 (^{o}C)
Absolute pressure (0-2067 kPa)	0.25% (full scale)
Differential pressure (0-10.0 kPa)	0.25% (full scale)
Differential pressure (0-37.4 kPa)	0.25% (full scale)
Mass flow rate	0.1% (reading)
Calculated Parameter	**Uncertainty**
Overall heat transfer coefficient	<2.5%
Friction factor	<8.7%

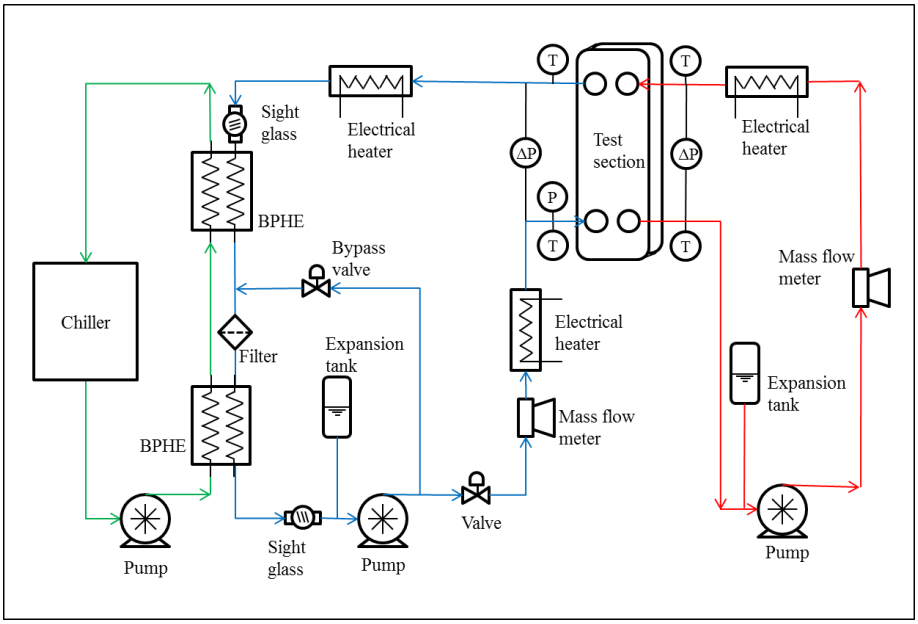

Figure 1: Schematics of experimental system

National Instrument SCXI1000 chassis is used for data acquisition. It is connected to a desktop computer through PCI-MIO-16e-1 and used in conjunction with LabVIEW software. The modules and terminal blocks used in the data logger are SCXI1102-SCXI1303 for input measurement and SCXI1124-SCXI1325 for output control. All data are obtained under steady state conditions for about 20 minutes.

The test section is well insulated, with heat loss calibrated so that the energy balance (measured heat load between hot and cold stream) is within ±3%, in accordance with ANSI/ASHRAE standard 181-2014 [15]. The geometries of the two types of heat exchangers tested are depicted in Figure 2. They are both of 1pass-1pass U-type configuration. The parameters of their geometry are summarized in Table 2.

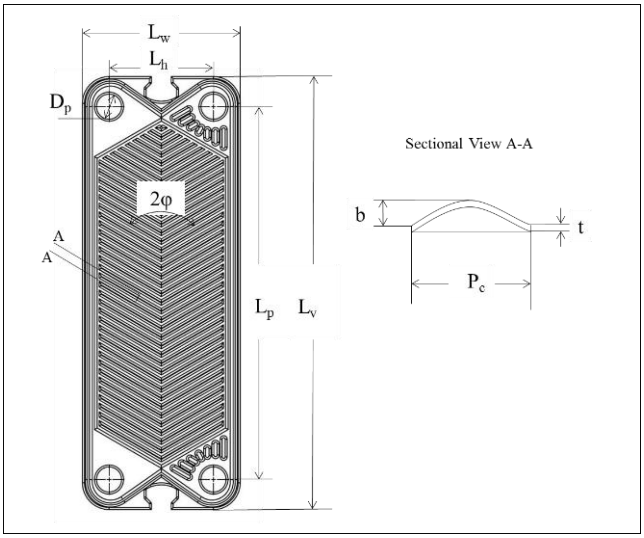

Figure 2: Schematics of heat exchanger plate

Table 2: Plate geometry of FPHE and BPHE

Parameter	FPHE	BPHE
Chevron angle, φ	60°	65°
Corrugation depth, b	2.20 mm	1.98 mm
Corrugation pitch, P_c	10.0 mm	7.4 mm
Plate thickness, t	0.60 mm	0.35 mm
Port length, L_p	495 mm	456 mm
Total length, L_v	578 mm	528 mm
Port width, L_h	140 mm	174 mm
Total width, L_w	210 mm	246 mm
Heat transfer area, A_{plate}	0.1017 m^2	0.1099 m^2
Port diameter, D_p	35.0 mm	47.8 mm

2.2 Data reduction

The primary measurements consist of the flow rates of each fluid stream, their inlet and outlet temperatures, and the pressure drop. Following the method outlined by Muley and Manglik [16], equivalent diameter D_e (=2*b*) is used for calculation with all relevant non-dimensional numbers (*Nu, Re,* etc.). Fluid properties are calculated at the bulk mean temperature given by

$$T_{h,b} = (T_{h,i} + T_{h,o})/2;\ T_{c,b} = T_{h,b} - LMTD \tag{1}$$

Where the LMTD is calculated by

$$LMTD = \left[(T_{h,i} - T_{c,o}) - (T_{h,o} - T_{c,i})\right] \Big/ \ln\left[(T_{h,i} - T_{c,o})/(T_{h,o} - T_{c,i})\right] \tag{2}$$

Since the number of channel of the hot side is always one larger or equal to the cold side and the mass fluxes are equal, $C_h \geq C_c$ prevails for all data points. As a result, Equation (1) and (2) is used to account for the nonlinear temperature variation and to agree with the characteristic wall temperature calculated from Equation (6).

The heat transfer is calculated from the average of hot side and cold side energy balance, whose difference is less than 3%.

$$Q_h = \dot{m} \cdot c_P \cdot [T_i - T_o]_h;\ Q_c = \dot{m} \cdot c_P \cdot [T_o - T_i]_c;\ Q_{avg} = (Q_h + Q_c)/2 \tag{3}$$

The overall heat transfer coefficient is calculated from Equation (4) and decomposed in the form of three thermal resistance in Equation (5). The wall temperature is determined iteratively through heat and resistance balance of Equation (6).

$$Q_{avg} = UA \cdot LMTD \tag{4}$$

$$(1/UA) = (1/h_h A_h) + (t/k_{plate} A_{plate}) + (1/h_c A_c) \tag{5}$$

$$Q_{avg} = h_h A_h (T_h - T_w) = (k_{plate} A_{plate}/t)(T_{w,h} - T_{w,c}) = h_c A_c (T_w - T_c) \tag{6}$$

Measured pressure drop is used to calculate the Fanning friction factor. The port losses, at both inlet and outlet of the heat exchanger for both fluids, are estimated based on empirical equation by Shah and Focke [17] in Equation (8). The pressure losses in the pipes between plates and measurement location, preceding or following the ports, are estimated on the basis of smooth tube friction factor.

$$\Delta P_{core} = \Delta P_{measured} - \Delta P_{port} - \Delta P_{pipe} \tag{7}$$

$$\Delta P_{port} = 1.5(\rho V_{port}^2/2) \tag{8}$$

The Fanning friction factor for a single channel is calculated through Equation (9). It is to be correlated with Re, as calculated by Equation (10).

$$f = \frac{\rho \cdot D_e \cdot \Delta P_{core}}{2L_P \cdot [\dot{m}/A_{cs}]^2}, \ D_e = 2b, A_{cs} \approx b \cdot L_w \tag{9}$$

$$\mathrm{Re} = \frac{(\dot{m}/A_{cs}) \cdot D_e}{\mu} \tag{10}$$

2.3 Experiment procedure

For each of the tested FPHE and BPHE, experiment was first conducted to characterize the isothermal friction factor by measuring adiabatic pressure drop in different mass flow rate in a single plate. The result will be shown discussed in the next section. The essence is to correlate the heat transfer coefficient in the same regime of turbulence so that one form of correlation would suffice.

Modified Wilson plot was used to correlate Nu as a power-law function of Re, Pr, and Sieter-Tate factor, as outlined by Shah [18]. For each data point, equal mass flux was maintained for both hot and cold stream. Since the fluid, geometry and mass flux are symmetric, the same Equation (11) is used for both hot and cold stream. The coefficients (C1, C2) were found through iterative linear regression for each tested heat exchanger.

$$Nu = C_1 \cdot \mathrm{Re}^{C2} \cdot \mathrm{Pr}^{1/3} \cdot (\mu/\mu_w)^{0.14} \tag{11}$$

The experiment was repeated for 2-channel (N=3) and 3-channel (N=4) setup for FPHE, each repeated with two compression forces of the frames by varying torque exerted on the bolts. Torque wrench was used to adjust the bolts with an increment of 0.565 N-m (5 in-lb.). Low compression platage was determined with the barely minimum torque required for sealing. Platage, defined as the distance between frames, was measured at locations of the six bolts. The average measured platage for high and low compression respectively were 10.49 mm and 11.15 mm for 2-channel, and 14.38 mm and 15.17 mm for 3-channel. For each low compression case, the change of platage per channel was added on the hydraulic diameter of the high compression case to reflect the change in cross sectional area.

As for the BPHE, a 2-channel (N=3), a 3-channel (N=4) and a 5-channel (N=6) BPHE was made by cutting the corresponding number of plates from an original BPHE and brazing the ports. Each was repeated with the same procedure of heat transfer test.

3. EXPERIMENTAL RESULTS AND DISCUSSION

3.1 Single-phase water friction factor

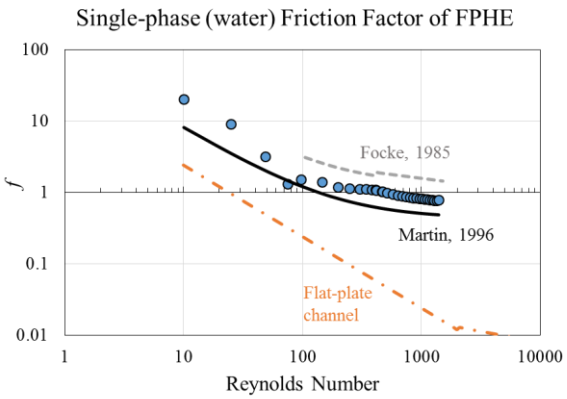

Figure 3: FPHE friction factor

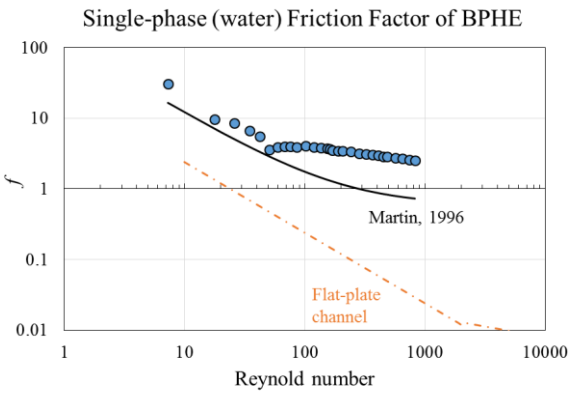

Figure 4: BPHE friction factor

As shown in Figure 3 and 4, friction factor shows an obvious transition in the trend around the Reynolds number of 100. Compared with *f* in equivalent flat plate as predicted by Kakac et al [19], the measured friction factor shows

much larger in value and lower Reynolds number in transition to turbulence. The transition to turbulence could happen from 10<Re<200, agrees with literature [20].

Similar trend was documented in many literatures, such as Focke [17], Martin [1] as compared in Figure 3. The difference in value may be attributed to the variation in the geometry, as pointed out by Muley and Manglik [16]. Instead of being a general correlation, the obtained friction factor was only a characterization of the plate used in this study. As a result, the heat transfer tests were performed in the same early turbulence regime, with 120<Re<500 For FPHE and 106<Re<226 for BPHE. The range of Pr tested are 4.1<Pr<6.0 for FPHE and 4.2<Pr<5.8 for BPHE.

3.2 Effect of end plate on heat transfer

As shown in in Figure 5 and 6, heat transfer is correlated for both hot (red) and cold (blue) stream with one curve fit in 2-channel and 3-channel PHE, for high and low compression. The goodness of fit R^2>0.99 for all cases.

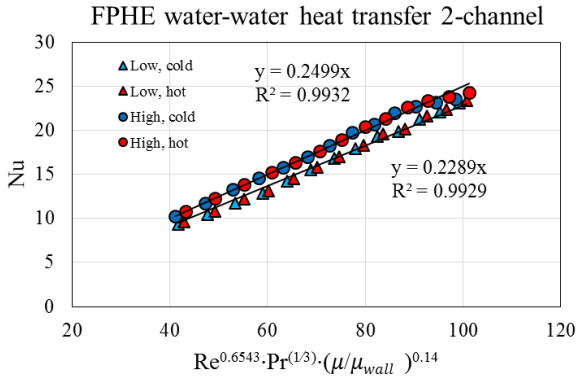

Figure 5: Correlation for 2-channel FPHE

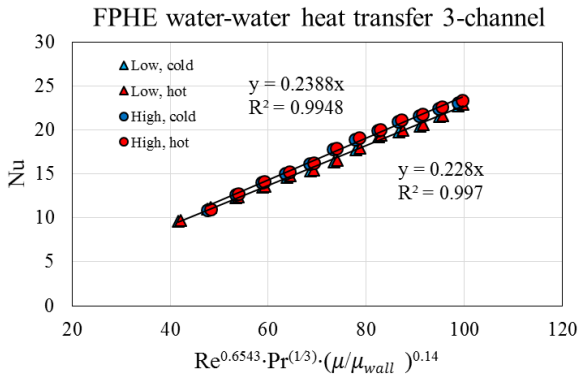

Figure 6: Correlation for 3-channel FPHE

A few observations are made for the four curve-fit. For low compression case, the heat transfer correlation in 2-channel and 3-channel almost overlap, with a difference less than 0.4%. While in high compression case, the difference is about 4.6%. In 2-channel FPHE, heat transfer coefficient in high compression case is about 9.2% higher than that in low compression case. In the 3-channel setup the difference is about 4.7%.

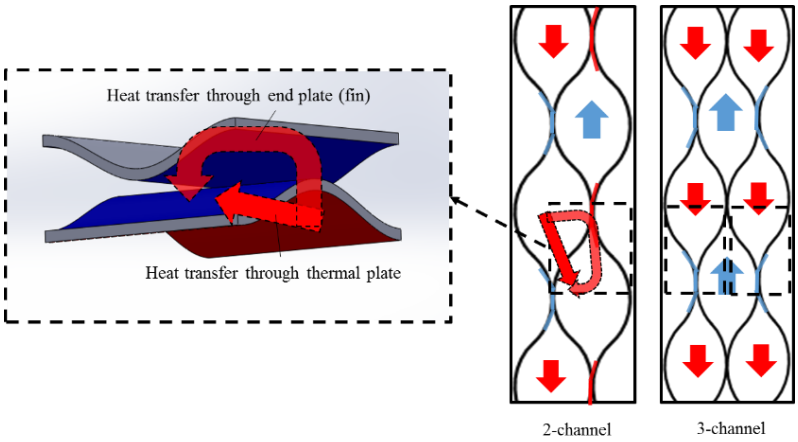

Figure 7: Schematics of heat transfer through thermal plate and end plate

The difference, although small, is non-trivial. It is attributed to the result of mistakenly treating the end plates as adiabatic, while in reality they act as fins and increase the effective heat transfer area through thermal conduction. At low compression, considering the elasticity of the gasket, the corrugated plates are barely in contact. Therefore fin efficiency is negligible, as supported by the same heat transfer correlation measured in both 2-channel and 3-channel. At high compression however, fin efficiency becomes more significant and it acts on the plates differently. As shown in Figure 7, in a 2-channel setup, both stream channels have one portion of surface enlargement. Whereas in a 3-

channel setup, the stream in the center channel does not have any enlargement while the stream in the two side channels, each having an end plate, receives two portions of enlargement. As a result, the heat transfer area should be corrected, as summarized in Table 3.

Table 3: Summary of correction with fin efficiency

Condition	A_c ideal	A_c corrected	A_h ideal	A_h corrected
2-channel high compression	A_{plate}	$(1+\eta)\ A_{plate}$	A_{plate}	$(1+\eta)\ A_{plate}$
2-channel low compression	A_{plate}	A_{plate}	A_{plate}	A_{plate}
3-channel high compression	$2A_{plate}$	$2A_{plate}$	$2A_{plate}$	$2(1+\eta)\ A_{plate}$
3-channel low compression	$2A_{plate}$	$2A_{plate}$	$2A_{plate}$	$2A_{plate}$

This concept could be extended to any number of plates as generalized in Equation (12) (hot stream in the two end channels for even number of plates).

$$\begin{aligned} &A_c = A_h = (N-2+\eta)A_{plate},\ N = 3,5,7... \\ &A_c = (N-2)A_{plate}, A_h = (N-2+2\eta)A_{plate},\ N = 4,6,8... \end{aligned} \tag{12}$$

Where the fin efficiency is defined as

$$\eta = Q_f\ /[hA_f(T_h - T_c)] = Q_f\ /[hA_{plate}(T_h - T_c)] \tag{13}$$

Substitute Equation (13) into Equation (5) to incorporate fin efficiency into the data reduction. Compare the data at each mass flux (high compression 2-channel vs. 3-channel, 2-channel high vs. low compression and 2-channel high vs. low compression) and solve for η, the relationship between fin efficiency and convective heat transfer is obtained, as plotted in Figure 11.

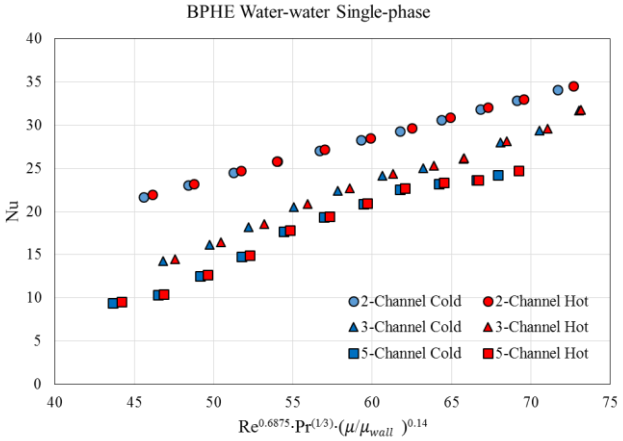

Figure 8: Heat transfer measured in BPHE

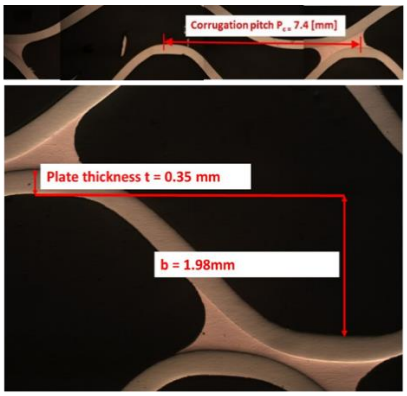

(Picture courtesy of Creative Thermal Solutions, Inc.)

Figure 9: Brazing joints of BPHE

Similarly, the measured heat transfer coefficient in BPHE for 2, 3 and 5 channels are plotted in Figure8. The results are correlated only with the area of thermal plates (are uncorrected). Therefore, heat transfer measured at the same condition in 2-channel BPHE has the highest value, since the highest percentage of area enlargement is neglected. Apply the same method of Equation (12) and (13) to calculate fin efficiency η as a function of heat transfer coefficient, as plotted in Figure 12. As a result, the fin efficiency in BPHE is much higher than that in the FPHE. The reason is due to the larger contact area and higher thermal conductivity of material at the brazing joints, as shown in Figure 9.

4. MODEL DESCRIPTION AND RESULTS

Due to the complexity of the geometry, it was difficult to obtain a theoretical solution of fin efficiency. A numerical model was developed in ANSYS to investigate the parameters of end-plate fin efficiency. The unitary cell of the exact geometry was created as shown in Figure 12, whose sinusoidal shape is described by Equation (14) and the parameters in Table 2.

$$f(x)=\frac{b}{2}\sin[\frac{2\pi}{P_c}(x-\frac{P_c}{4})]+\frac{b}{2} \tag{14}$$

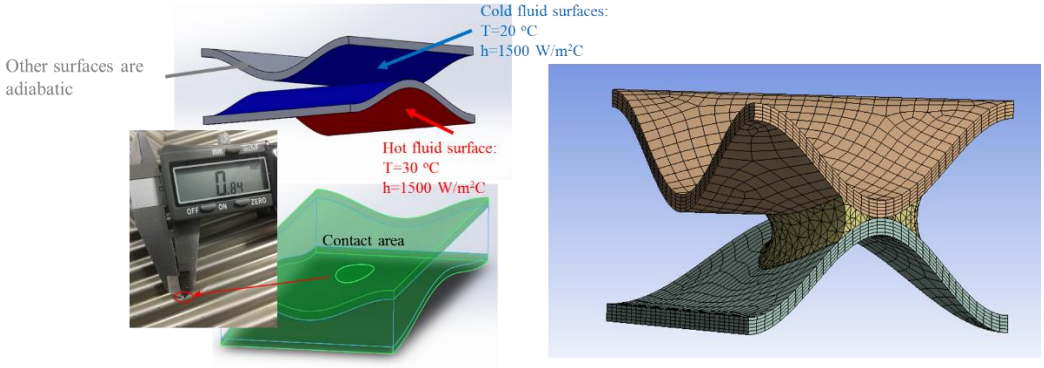

Figure 10: Schematics of FPHE unitary cell and boundary conditions (left) and meshed BPHE cell (right)

A lumped convective heat transfer coefficient and fluid temperature was applied to both fluid surfaces as boundary conditions. The other surfaces were adiabatic. Heat transfer coefficient was set the same for both streams and parameterized to investigate its effect. The fluid temperature was fixed at 30 °C for the hot stream and 20 °C for the cold stream, since the temperature difference would eventually be cancelled out upon solving fin efficiency and its value only has negligible effect in the material conductivity in the operating range. The plate material is stainless steel 316. In the BPHE model, the brazing material is copper and its geometry was created according to Figure 9. In FPHE model, the contact surface was set as "bond" type (no relative motion) and the contact resistance was lumped into the change of the area. The modeled area varied from 0.34 mm^2 to 3.49 mm^2. As a simplification, the model did not concern any deformation of the plate. Sensitivity analysis for node number was conducted, at node number of 110426, 195460 and 224426, the difference in result is less than 0.1%. A node number of 224426 is used for this study.

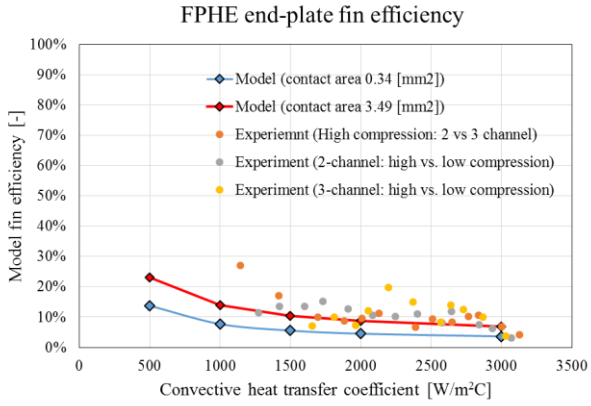

Figure 11: FPHE end plate fin efficiency

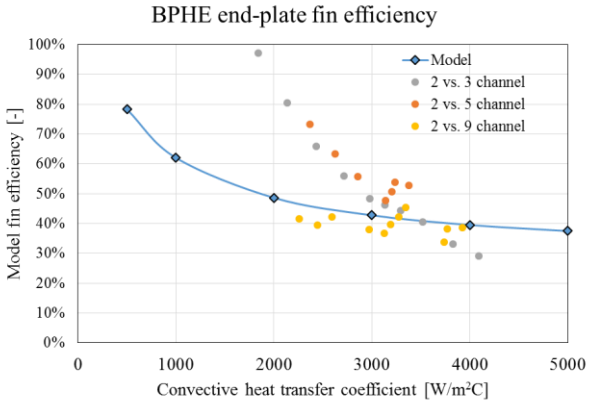

Figure 12: BPHE end plate fin efficiency

The model outputs the total heat transfer, which is used together with the boundary conditions of fluid temperature and heat transfer coefficient in Equation (4), (5), (6), (12) and (13) to solve for fin efficiency. The results are plotted in Figure 11 and 12 in comparison with the experimental data. It is observed that the model agrees with experiments in general trend that the fin efficiency decreases with convective heat transfer coefficient. As expected, with larger contact area or smaller contact resistance, the fin efficiency is larger. The values have better agreement at higher heat

transfer coefficient. At lower heat transfer coefficient, the discrepancy may have been caused by two reasons. One is the simplification of a lumped fluid heat transfer coefficient, as the heat transfer coefficient in unitary cell has been shown to vary by experiment [21-22] and CFD model [22-23]. The other reason is that the experimental data only represents an averaged value of the entire heat exchanger. At lower heat transfer coefficient (mass flow rate), the disparity of heat transfer coefficient at inlet and outlet caused by fluid temperature is more significant.

5. CONCLUSIONS

This paper presents experimental data and numerical model to illustrate that end plates in both frame-and-plate (FPHE) and brazed plate heat exchangers (BPHE) function as fin. The model, using a lumped boundary conditions, represents the trend of experimental data, with better agreement at higher convective heat transfer coefficient. The fin efficiency decreases with heat transfer coefficient and increases with contact area. As a result, end plate effect is stronger in BPHE due to the larger contact area and higher conductivity of the brazing material. The effect of end plates is quickly diluted by the increased number of plates in real applications, but it could be significant when plate number is small, as is often the case in laboratory settings for the development of heat transfer correlations. The result of fin efficiency as a function of heat transfer coefficient could then be used to iteratively correct the measurement.

NOMENCLATURE

A	Area	m^2	Re	Reynolds number	
b	Plate thickness	mm			
C	Heat capacitance		**Subscripts**		
Cp	Specific heat	kJ/kg-K	avg	average	
f	Fanning friction factor		b	bulk	
D_e	Equivalent diameter	m	c	cold	
G	Mass flux	kg/m^2s	cs	cross section	
h	Heat transfer coefficient	W/m^2-K	f	fin	
k	Conductivity	W/m-K	h	hot	
L	length	mm	i	inlet	
m	Mass flow rate	kg/s	o	outlet	
N	Number of plates				
Nu	Nusselt number		**Greek Letters**		
NTU	Number of transfer unit		ε	Effectiveness	
P	Pressure	kPa	ρ	Density	kg/m^3
Pr	Prandtl number		μ	Dynamic viscosity	kg/m-s
Q	Capacity	kW	φ	Corrugation angle	^{o}

REFERENCES

[1] Martin, H. (2010). Pressure drop and heat transfer in plate heat exchangers, VDI Heat Atlas, Springer Science & Business Media

[2] Abu-Khader, M. M. (2012). Plate heat exchangers: recent advances. Renewable and Sustainable Energy Reviews, 16, 1883-1891.

[3] Wang, L., Sunden, B., & Manglik, R. M. (2007), *Plate Heat Exchangers: Design, Applications and Performance*, WIT Press; 1st edition

[4] Kandlikar, S. G., & Shah, R. K. (1989). Multipass Plate Heat Exchangers—Effectiveness-NTU Results and Guidelines for Selecting Pass Arrangements. Journal of heat transfer, 111(2), 300-313. doi: 10.1115/1.3250678

[5] Heggs, P.J. & Scheidat, H.J. (1992), Thermal Performance of Plate Heat Exchanger with Flow Maldistribution, *Compact Heat Exchangers for Power and Process Industries*, ed. R.K. Shah, T.M. Rudy, J.M. Robertson, and K.M. Hostetler, HTD, vol 201, ASME, New York, pp. 87-93

[6] Buonopan, R.A., Troupe, R.A. & Morgan, J.C. (1961), Heat transfer design method for plate heat exchanger, *Chem. Engg. Prog.*, No.7, 59, pp.57-61

[7] Foote, M, R., (1967), Effective mean temperature difference in multipass heat exchanger, *NEL Report No. 303*, National Engineering Lab, Glasgow, United Kingdom.
[8] Usher, J.D. (1969), The plate heat exchanger in compact heat exchanger, *NEL Report No. 482*, National Engineering Lab, Glasgow, U.K.
[9] Marriott, J., (1971), Where and How to Use Plate Heat Exchangers, *Chemical Engineering*, Vol. 78, No. 8, pp. 127-133.
[10] Jackson, B.W. & Troupe, R.A. (1966), Plate exchanger design by ε-NTU method, *Chem. Engg. Prog. Symp.* Series No.64, 62 185-190.
[11] Kandlikar, S. (1984), Performance curve for different plate heat exchanger configuration, *ASME Paper* No.84-HT-26.
[12] Polley, G. T. & Abu-Khader, M. M (2005), Compensating for end effects in plate-and-frame heat exchangers, *Heat transfer engineering*, 26(10):3–7, doi: 10.1080/01457630500248471
[13] Yan, Y.-Y., & Lin, T.-F. (1999). Evaporation heat transfer and pressure drop of refrigerant R-134a in a plate heat exchanger. *Transactions of the SAME*, 121, 118-127.
[14] Yan, Y.-Y., Lio, H.-C., & Lin, T.-F. (1999). Condensation heat transfer and pressure drop of refrigerant R-134a in a plate heat exchanger. *International Journal of Heat and Mass Transfer*, 42(6), 993-1006. doi: http://dx.doi.org/10.1016/S0017-9310(98)00217-8
[15] ASHRAE standard 181-2014, Methods of testing for rating liquid-to-liquid heat exchangers,
[16] Muley, A., & Manglik, R. M. (1999). Experimental Study of Turbulent Flow Heat Transfer and Pressure Drop in a Plate Heat Exchanger With Chevron Plates. *Journal of* heat transfer, 121(1), 110-117. doi: 10.1115/1.2825923
[17] Focke, W. W., Zachariades, J., & Olivier, I. (1985). The effect of the corrugation inclination angle on the thermohydraulic performance of plate heat exchangers. International Journal of Heat and Mass Transfer, 28(8), 1469-1479. doi: http://dx.doi.org/10.1016/0017-9310(85)90249-2
[18] Shah, R. K. (1990). Assessment of modified Wilson plot techniques for obtaining heat exchanger design data Heat Transfer, *Proceedings of the International Heat Transfer Conference*.
[19] Kakac, S., Shah, R. K., & Aung, W. (1987), *Handbook of Single-Phase Convective Heat Transfer*, John Wiley and Sons, New York.
[20] Shah, R.K. & Sekulic, D.P. (2002), *Fundamentals of heat transfer design*, Wiley; 1 edition
[21] Stasiek, J., Collins, M. W., Ciofalo, M., & Chew, P. E. (1996). Investigation of flow and heat transfer in corrugated passages—I. Experimental results. International Journal of Heat and Mass Transfer, 39(1), 149-164. doi: http://dx.doi.org/10.1016/S0017-9310(96)85013-7
[22] Freund, S., & Kabelac, S. (2010). Investigation of local heat transfer coefficients in plate heat exchangers with temperature oscillation IR thermography and CFD. International Journal of Heat and Mass Transfer, 53(19–20), 3764-3781. doi: http://dx.doi.org/10.1016/j.ijheatmasstransfer.2010.04.027
[23] Etmad, S. & Sunden, B. (2007), CFD-analysis of fully developed turbulent flow and heat transfer in a unitary cell of a cross corrugated plate pattern heat exchanger. *Proceedings of HT2007, ASME-JSME Thermal Engineering Summer Heat Transfer Conference,* Vancouver, British Columbia, Canada

ACKNOWLEDGEMENT

The authors thankfully acknowledge the support provided by the Creative Thermal Solutions, Inc. and Air Conditioning and Refrigeration Center at the University of Illinois at Urbana-Champaign. The authors also gratefully thank research assistant Fiona Y. Zang for her contribution of lab work.